A study on application of high strength steel SM570 in bridge piers with stiffened box section under cyclic loading

Lan Kang [1,3a], Motoya Suzuki [2] and Hanbin Ge [*2]

[1] *School of Civil Engineering and Transportation, South China University of Technology, Guangzhou, 510640, China*
[2] *Department of Civil Engineering, Meijo University, Nagoya, 468-8502, Japan*
[3] *State Key Laboratory of Subtropical Building Science, South China University of Technology, Guangzhou, Guangdong Province, 510641, China*

Abstract. Although a lot of experimental and analytical investigations have been carried out for steel bridge piers made of SS400 and SM490, the formulas available for SS400 and SM490 are not suitable for evaluating ultimate load and deformation capacities of steel bridge piers made of high strength steel (HSS) SM570. The effect of various parameters is investigated in this paper, including plate width-to-thickness ratio, column slenderness ratio and axial compression force ratio, on the ultimate load and deformation capacities of steel bridge box piers made of SM570 steel subjected to cyclic loading. The elasto-plastic behavior of the steel bridge piers under cyclic loads is simulated through plastic large deformation finite element analysis, in which a modified two-surface model (M2SM) including cyclic hardening is employed to trace the material nonlinearity. An extensive parametric study is conducted to study the influences of structural parameters on the ultimate load and deformation capacities. Based on these analytical investigations, new formulas for predicting ultimate load and deformation capacities of steel bridge piers made of SM570 are proposed. This study extends the ultimate load and deformation capacities evaluation of steel bridge piers from SS400, SM490 steels to SM570 steel, and provides some useful suggestions.

Keywords: steel bridge pier; ultimate load; deformation capacity; high strength steel; two-surface model

1. Introduction

With the development of the steel production and manufacture process, high strength steel (HSS) structures have been increasingly applied to building and bridge constructions in recent years, due to their advantages in structural safety, architectural function, economical benefit and resource saving etc (Coelho and Bijlaard 2010, Yan *et al.* 2014, Guo *et al.* 2015, Joo *et al.* 2015, Bradford and Liu 2016, Ma *et al.* 2016). Meanwhile, with the development of steel technology, the cost of HSS structures will be greatly reduced (Wang *et al.* 2015). Flexural behaviors of HSS beams have been fully studies by some researchers (Wang *et al.* 2016, Wang and Gardner 2017). Furthermore, some previous studies focused on the ultimate load capacity, local buckling and global buckling behaviors of HSS columns under axial compression. First of all, the ultimate load evaluation of HSS unstiffened columns are studies by some researchers. Load-carrying capacity of HSS box columns subjected to axial compression was experimentally obtained, and a novel prediction equation evaluating its ultimate load was proposed by Gao *et al.* (2009). Buckling strength of Q420 HSS angle columns was obtained through tests and simulations by Cao *et al.* (2015). The behavior of

HSS columns under combining vertical load and lateral load was studies by Gkantou *et al.* (2017). Secondly, the local and global buckling behaviors of HSS columns were investigated experimentally and analytically. The local buckling behavior of Q420 equal angle columns and Q960 welded box columns were experimentally and numerically investigated in some previous studies (Shi *et al.* 2012, 2014, 2015). The global buckling behaviors of Q690 welded box and H-shape columns were investigated on twelve axially compression specimens by conducting test and finite element analysis (Li *et al.* 2016a, b), and the tested results were compared with current standards. The global buckling performance of Q960 steel columns was studied by some researchers (Ban *et al.* 2013a, c). A total of 30 HSS square and rectangular hollow section columns were tested to obtain their flexural buckling behavior (Wang and Gardner 2017). Besides, the residual stress distributions of HSS welded columns with both box and H-shape sections were obtained based on experimental results in some references (Chiew *et al.* 2012, Ban *et al.* 2013b, Khan *et al.* 2016). However, small yield ratio and small elongation of HSS may be not good for the seismic performance of HSS members, and such these properties of HSS may prevent its application in seismic area. Thus, it is important and necessary to fully and deeply study the hysteretic behavior of HSS members, especially HSS bridge piers.

A lot of experimental and theoretical studies on seismic behavior of normal strength steel (NSS) columns have been conducted in previous studies (Kumar and Usami 1996, Ge *et al.* 2000, Usami *et al.* 2000, Aoki and Susantha 2005,

---

∗Corresponding author, Professor,
 E-mail: gehanbin@meijo-u.ac.jp
[a] Associate Professor, E-mail: ctlkang@scut.edu.cn

Nakashima and Liu 2005, Wang and Yamao 2011, Li *et al.* 2017, Liao *et al.* 2017). Besides, some researchers evaluated the seismic performance of HSS columns. Seismic tests of concentrically braced steel frame buildings with high strength tubular steel columns were carried out by Ferrario *et al.* (2016). Chen *et al.* (2016) conducted cyclic loading test and numerical simulation of Q690D HSS H-section columns in order to evaluate hysteretic performance of HSS columns. Six Q460 HSS columns were tested under constant axial load and cyclic horizontal load by Wang *et al.* (2014a). The seismic performance of welded box- and H-section beam-columns with nominal yield strength of 460 MPa were evaluated by Wang *et al.* (2014b). These experimental results illustrated that the seismic performances of HSS members differ from those of NSS members under cyclic loading. However, these studies concentrated on unstiffened HSS columns, not stiffened HSS members, which begin to be applied in long span bridge structures (Wang and Yamao 2011). The seismic behavior of HSS stiffened structures under cyclic loading still is unresolved, and further research is needed.

This study is aimed to investigate an application of HSS SM570 to bridge piers and to evaluate the ultimate load and deformation capacities of steel bridge piers with stiffened box section under cyclic loads. In the present numerical research, the modified two-surface model (M2SM) is employed to describe material nonlinearity. Moreover, the effect of steel type on the cyclic plastic behavior of steel bridge piers is studied first. Then, an extensive parametric study is conducted to investigate the effects of the width-to-thickness ratio, slenderness ratio, axial compression force ratio on the ultimate load and deformation capacities of the steel bridge piers under cyclic loadings. Furthermore, some formulas are proposed to predict the ultimate load and deformation capacities of stiffened steel bridge box piers.

2. Analytical model

2.1 Finite element model of steel bridge piers

In order to investigate influences of main parameters on the seismic behavior of stiffened steel bridge piers, 24 columns are analyzed by employing the general finite element software ABAQUS. Finite element models of steel bridge piers with stiffened box section are illustrated in Fig. 1. Stiffened cross section for the lower part where local buckling may occur and equivalent unstiffened cross section for upper part of analytical steel bridge piers are shown in Fig. 2, respectively. The stiffened sections are transformed into equivalent unstiffened sections by defining the equivalent flange and web thickness, $\bar{t}_f$ and $\bar{t}_w$ for the beam element. Detailed description of this transformation can be found in the reference (Zheng *et al.* 2000). What's more, a large deformation finite element analysis procedure is done to examine the behavior of columns subjected to lateral cyclic loads (as shown in Fig. 3).

The $2B$ or $3l_d$ lower part of the column specimens is simulated by employing 4-node reduced integrated thin shell element of S4R. In which, B is the flange width and l_d is the distance between diaphragms. For analytical model with stiffened box sections, aspect ratio of the flange plate between two diaphragms (i.e., ratios of distance between diaphragms to flange width) is 0.5. The beam-column element of B31 based on Timoshenko beam theory is employed to simulate the upper part of column.

2.2 Structural parameters and cyclic material model

The geometric dimensions and structural parameters of 24 steel bridge piers are listed in Table 1. In this paper, a total of five parameters, such as width-to-thickness ratio (R_f), column slenderness ratio ($\bar{\lambda}$), stiffener's equivalent
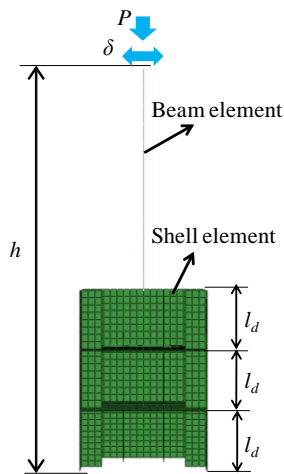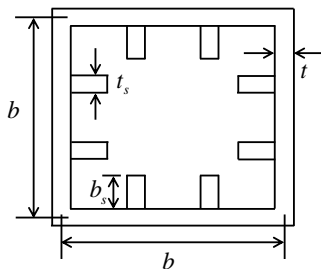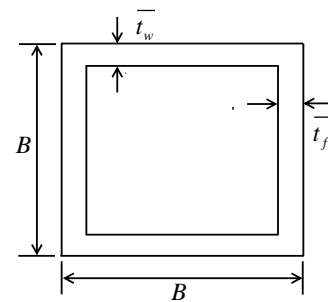

Fig. 1 Analytical model of steel bridge piers

(a) Stiffened cross section for shell element part

(b) Equivalent unstiffened cross section for beam element part

Fig. 2 Cross section

slenderness ratio ($\bar{\lambda}_s$), axial compression force ratio (P/P_y), and material type of steel columns, are taken into account.

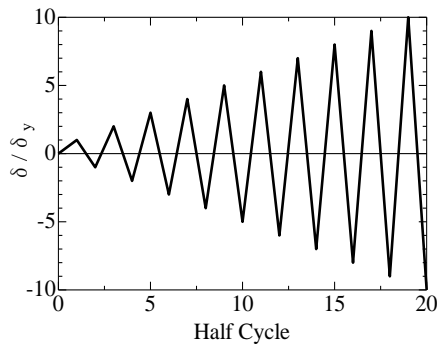

Fig. 3 Cyclic loading pattern

These five parameters are also the main parameters considered in the practical design (Ge *et al*. 2000, Usami *et al*. 2000). In which, the structural parameters, including the width-to-thickness ratio and slenderness ratio, can be obtained as follows (Ge *et al*. 2000, Usami *et al*. 2000, Ge and Kang 2012)

$$R_f = \frac{b}{t}\sqrt{\frac{\sigma_y}{E}\frac{12(1-v^2)}{\pi^2 k}} \tag{1}$$

$$\bar{\lambda} = \frac{Kh}{r}\frac{1}{\pi}\sqrt{\frac{\sigma_y}{E}} \tag{2}$$

where *b* stands for the flange width measured from plate thickness centerlines, *t* is the flange thickness, *E* represents the Young's modulus, *v* is the Poisson's ratio and σ_y

Table 1 Geometric dimensions and structural parameters of analytical steel bridge piers

No.	R_f	$\bar{\lambda}$	$\bar{\lambda}_s$	γ/γ^*	α	h (mm)	b (mm)	t (mm)	b_s (mm)	t_s (mm)	B (mm)	$\bar{t_f}$ (mm)	$\bar{t_w}$ (mm)	P/P_y	H_y (MN)	δ_y (mm)	Steel type
1		0.25				2090									2.17	8.00	
2	0.25	0.35	0.149			2926	625		92		645	22.30	29.99		1.55	15.67	
3		0.45				3762									1.21	25.91	
4		0.25				2968									2.95	11.62	
5	0.35	0.35	0.207			4156	875		101		895	22.08	27.38	0.15	2.11	22.78	
6		0.45				5343									1.64	37.66	
7		0.25				3846									3.72	15.25	
8	0.45	0.35	0.272			5384	1125		108		1145	21.86	25.95		2.66	29.89	
9		0.45				6922									2.07	49.42	SM570
10		0.25				2090									1.79	6.59	
11	0.25	0.35	0.149			2926	625		92		645	22.30	29.99		1.28	12.91	
12		0.45		3.0	0.50	3762		20		20					0.99	21.34	
13		0.25				2968									2.43	9.57	
14	0.35	0.35	0.207			4156	875		101		895	22.08	27.38	0.30	1.74	18.76	
15		0.45				5343									1.35	31.02	
16		0.25				3846									3.06	12.56	
17	0.45	0.35	0.272			5384	1125		108		1145	21.86	25.95		2.19	24.62	
18		0.45				6922									1.70	40.70	
19	0.25		0.147			4027	731		97		751	22.21	28.72		1.07	18.67	
20	0.35		0.204			5707	1023		106		1043	21.95	26.49	0.15	1.45	26.98	
21	0.45	0.35	0.269			7385	1315		113		1335	21.74	25.26		1.84	35.29	SM490
22	0.25		0.147			4027	731		97		751	22.21	28.72		0.88	15.37	
23	0.35		0.204			5707	1023		106		1043	21.95	26.49	0.30	1.20	22.22	
24	0.45		0.269			7385	1315		113		1335	21.74	25.26		1.51	29.06	

*Notes: R_f = width-to-thickness ratio, $\bar{\lambda}$ = column slenderness ratio, $\bar{\lambda}_s$ = stiffener's equivalent slenderness ratio, γ/γ^* = stiffness ratio of stiffeners (in which γ = stiffness of longitudinal stiffeners, γ^* = optimum stiffness of longitudinal stiffeners calculated by linear buckling theory), α = aspect ratio of the flange plate between two diaphragms (l_d/b, l_d = spacing between two transverse stiffeners), h = column height, b = flange width measured from web plate thickness centerlines, equal to web height measured from flange plate thickness centerlines, t = flange thickness, b_s = width of stiffener, t_s = thickness of stiffener, $B = b + t$, $\bar{t_f}$ = equivalent flange thickness, $\bar{t_w}$ = equivalent web thickness, P/P_y = axial compression force ratio (where the axial yield force P_y is computed when the full cross section is in plasticity)
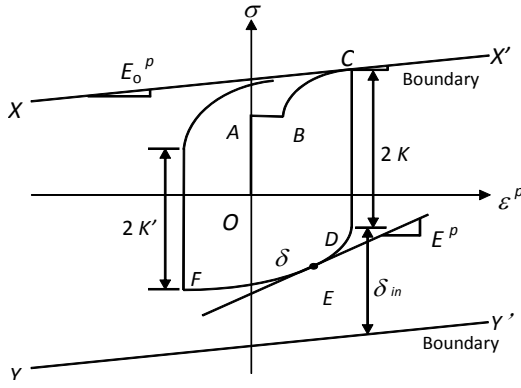
Fig. 4 Modified two-surface model
(Shen *et al.* 1995, JRA 2002)

represents the yield stress, k is the buckling coefficient of a plate (= $4n^2$, n is the number of subpanels in each plate panel. In this study, $n = 3$ for a section shown in Fig. 2), h is the column height, r is the radius of gyration of cross section, (= $\sqrt{I/A}$), A is the area of cross section, I is the cross sectional moment of inertia, and K represents the effective length factor. The stiffness of longitudinal stiffeners (γ) and the optimum stiffness of longitudinal stiffeners (γ^*) can be obtained based on linear buckling theory.

$$\gamma = \frac{t_s b_s^3 / 3}{bt^3 / 11} \tag{3}$$

$$\gamma^* = 4\alpha^2 n \left(1 + n \frac{b_s t_s}{bt}\right) - \frac{(\alpha^2 + 1)^2}{n} \tag{4}$$

where b_s = width of stiffener, t_s = thickness of stiffener, $\alpha = l_d/b$, aspect ratio of the flange plate between two diaphragms, in which, l_d = spacing between two transverse stiffeners. The slenderness ratio of stiffeners can be described as follows

$$\bar{\lambda}_s = \frac{1}{\sqrt{Q}} \frac{l_d}{r_s} \frac{1}{\pi} \sqrt{\frac{\sigma_y}{E}} \tag{5}$$

where r_s is the radius of gyration of T-shaped cross section, and Q stands for the local buckling strength of sub-panels surrounded by longitudinal stiffeners, which can be defined as follows

$$Q = \frac{1}{2R_f} \left[\beta - \sqrt{\beta^2 - 4R_f}\right] \leq 1.0 \tag{6}$$

$$\beta = 1.33R_f + 0.868 \tag{7}$$

The constitutive law of M2SM (Mamaghani *et al.* 1995, Shen *et al.* 1995) (as shown in Fig. 4) developed by Nagoya University is employed, which is a satisfactory model for evaluating the cyclic hysteretic behavior of both thin- and thick-walled steel bridge box piers. The corresponding material parameters can be obtained from the recommended

Table 2 Material properties and model parameters of SM490 and SM570 (Shen *et al.* 1995)

Steel type	SM490	SM570
Young's modulus E (MPa)	206000	216000
Initial strain hardening modulus E_{st}^p (MPa)	7004	4363.2
Yield stress σ_y (MPa)	315	450
Poisson ratio v	0.30	0.30
Strain at the onset of strain hardening ε_{st}	0.00918	0.004167
Initial value of boundary's slope $E_{0,in}^p$ (MPa)	2080.6	1695.6
Size of initial elastic range k_0 (MPa)	355.95	477
Parameter e	306	700
Parameter f	99704	77976
Parameter a	-0.528	-0.553
Parameter b	1.88	6.47
Parameter c	18.7	34.8
Parameter α	0.217	0.175
Parameter M	-0.522	0
Extreme value of elastic range k_∞ (tensile strength σ_u) (MPa)	507.15	549
Parameter ζ	650.07	1852.416
Parameter ω (mm²/N)	0.0127	0.005933

values of steel materials (including SM490 and SM570) in the reference (JRA 2002), as given in Table 2.

3. Analytical results of parametric study

To investigate effects of the steel type, width-to-thickness ratio, column slenderness ratio and axial compression force ratio on the seismic behavior of steel bridge piers, 24 steel bridge piers are modeled and analyzed. The scopes of parameters considered are two steel types of SM570 and SM490, $R_f = 0.25 - 0.45$, $\bar{\lambda} = 0.25 - 0.45$, and $P/P_y = 0.15 - 0.30$.

3.1 Effect of steel type (SM570 and SM490)

First of all, Fig. 5 demonstrates hysteresis curves of steel bridge piers made of SM570 (No. 5 in Table 1) and SM490 (No. 20 in Table 1), which have the same width-to-thickness ratio, slenderness ratio and axial compression force ratio ($R_f = 0.35$, $\bar{\lambda} = 0.35$, $P/P_y = 0.15$). After obtaining the lateral load-lateral displacement curve (as shown in Fig. 5(a)), the yield lateral load, H_y, and yield lateral displacement, δ_y, will be employed to non-dimensionalize the curves (as shown in Fig. 5(b)). Here, H_y is taken as the smaller one from the following two equations (Usami and Ge 1998)

$$H_y = \frac{M_y}{0.85h}\left(1 - \frac{P}{P_E}\right)\left(1 - \frac{P}{P_u}\right) \tag{8}$$
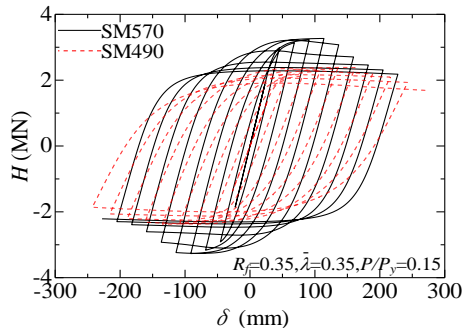
(a) Lateral load-lateral displacement hysteretic curve
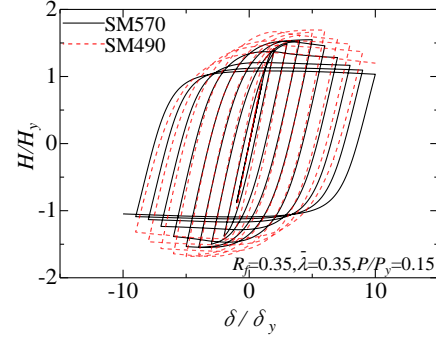
(b) Dimensionless lateral load-lateral displacement hysteretic curve

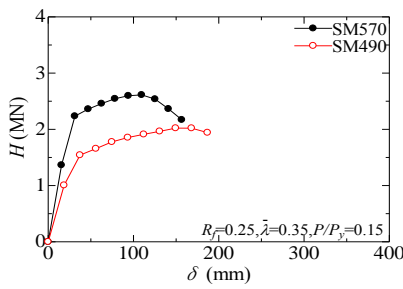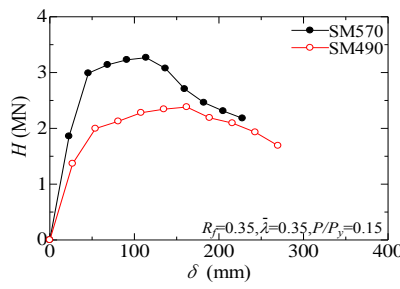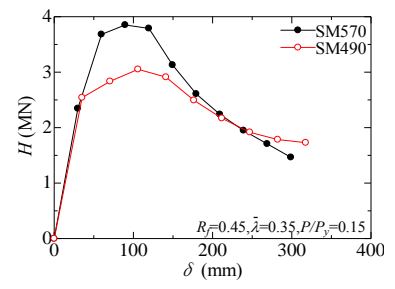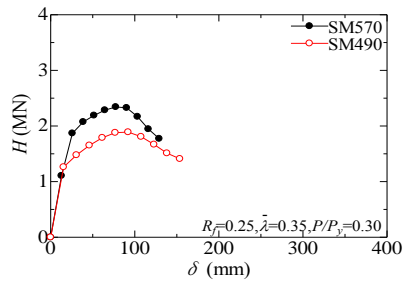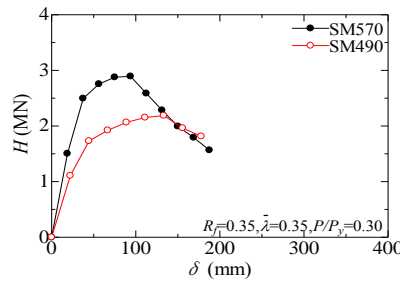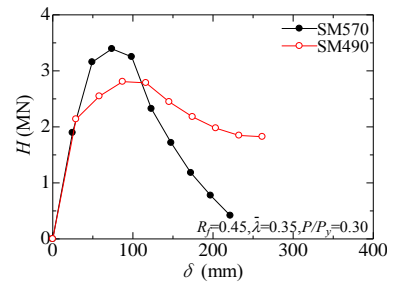Fig. 5 Effect of steel type on seismic performance of steel bridge piers

(a) $R_f = 0.25,\ \bar{\lambda} = 0.35,\ P/P_y = 0.15$

(b) $R_f = 0.35,\ \bar{\lambda} = 0.35,\ P/P_y = 0.15$

(c) $R_f = 0.45,\ \bar{\lambda} = 0.35,\ P/P_y = 0.15$

(d) $R_f = 0.25,\ \bar{\lambda} = 0.35,\ P/P_y = 0.30$

(e) $R_f = 0.35,\ \bar{\lambda} = 0.35,\ P/P_y = 0.30$

(f) $R_f = 0.45,\ \bar{\lambda} = 0.35,\ P/P_y = 0.30$

Fig. 6 Effect of plate steel type on lateral load-lateral displacement envelope curves

$$H_y = \frac{M_y}{h}\left(1 - \frac{P}{P_y}\right) \qquad (9)$$

$$\delta_y = \frac{H_y h^3}{3EI} \qquad (11)$$

where M_y = yield moment of cross section; P_E = Euler's buckling load of a cantilever column; P_u = ultimate load of centrally loaded column, which is determined from the following equation adopted in the Japanese specification for road bridges (JRA 2002).

$$\frac{P_u}{P} = \begin{cases} 1.0 & \left(\bar{\lambda} \le 0.2\right) \\ 1.109 - 0.545\bar{\lambda} & \left(0.2 \le \bar{\lambda} \le 1.0\right) \\ 1/\left(0.773 + \bar{\lambda}^2\right) & \left(\bar{\lambda} \ge 1.0\right) \end{cases} \qquad (10)$$

The yield lateral displacement, δ_y, can be calculated as followed equation without considering the effect of transverse shear deformation

From the dimensionless hysteretic curves in Fig. 5(b), it is illustrated that the ultimate load capacity and deformation capacity of steel bridge pier made of SM570 is almost equal to those of steel bridge pier made of SM490. However, the following important observation can be made from the dimensional hysteretic curves in Fig. 5(a) that the ultimate load of steel bridge pier made of SM570 is approximately 1.33 times that of steel bridge pier made of SM490. Furthermore, the same results can be obtained from the other comparisons between analytical cases (such as No. 2 and No. 19, No. 8 and No. 21, No. 11 and No. 22, No. 14 and No. 23, No. 17 and No. 24).

Besides, it is observed from Fig. 6 that the steel bridge piers made of SM570 have better deformation capacity. From the view of energy absorption, different conclusions may be made. Table 3 lists the energy absorption of steel
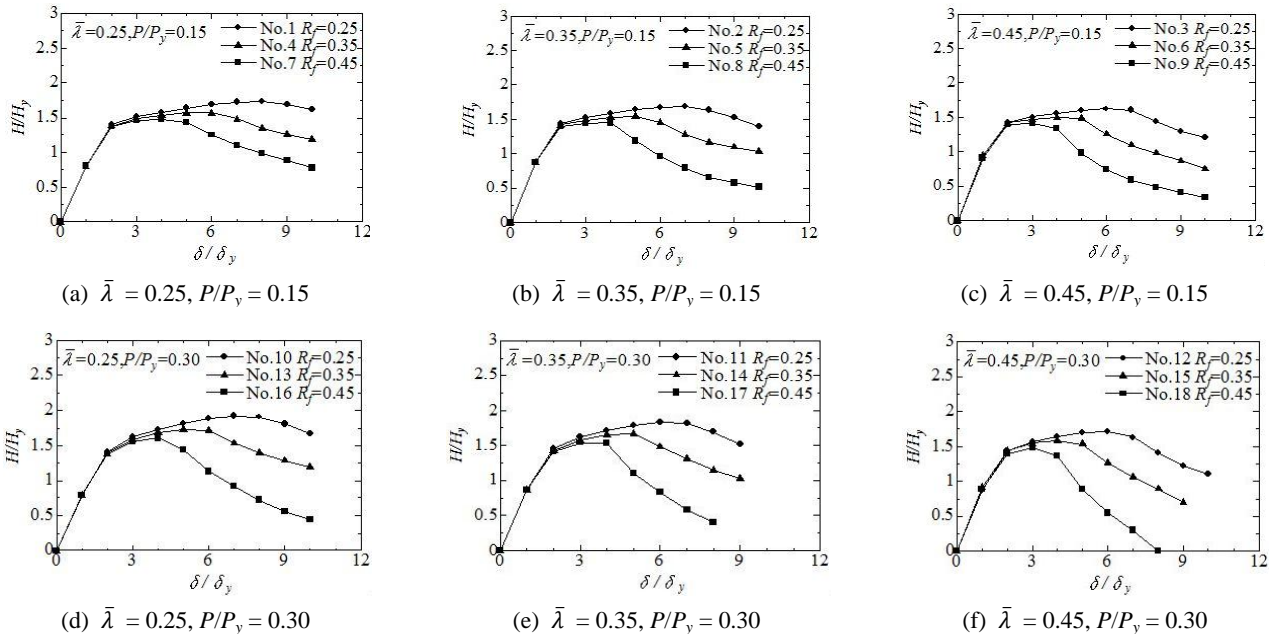
(a) $\bar{\lambda} = 0.25$, $P/P_y = 0.15$ (b) $\bar{\lambda} = 0.35$, $P/P_y = 0.15$ (c) $\bar{\lambda} = 0.45$, $P/P_y = 0.15$

(d) $\bar{\lambda} = 0.25$, $P/P_y = 0.30$ (e) $\bar{\lambda} = 0.35$, $P/P_y = 0.30$ (f) $\bar{\lambda} = 0.45$, $P/P_y = 0.30$

Fig. 7 Effect of column width-to-thickness ratio on lateral load-lateral displacement envelope curves

(a) $R_f = 0.25$, $P/P_y = 0.15$ (b) $R_f = 0.35$, $P/P_y = 0.15$ (c) $R_f = 0.45$, $P/P_y = 0.15$

(d) $R_f = 0.25$, $P/P_y = 0.30$ (e) $R_f = 0.35$, $P/P_y = 0.30$ (f) $R_f = 0.45$, $P/P_y = 0.30$
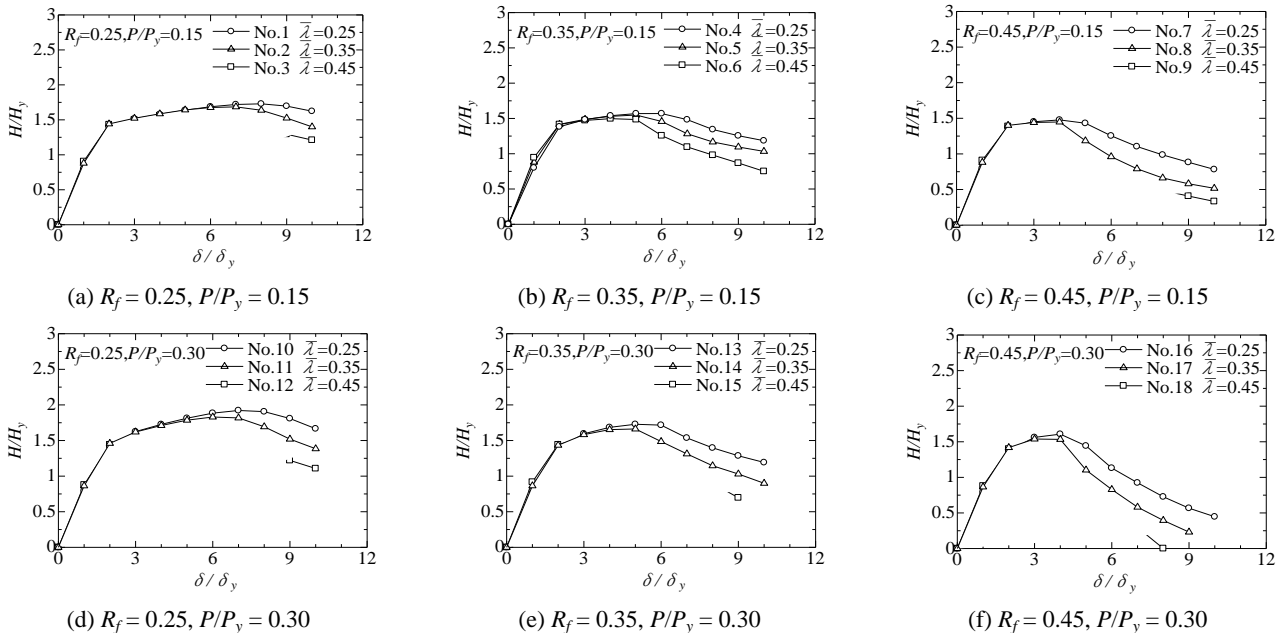
Fig. 8 Effect of slenderness ratio on lateral load-lateral displacement envelope curves

Table 3 Energy absorption of steel bridge piers made of SM570 and SM490

R_f	$\bar{\lambda}$	P/P_y	Energy absorption (MJ)			
			Ultimate load		95% of ultimate load	
			SM570	SM490	SM570	SM490
0.25			171.8	182.2	171.9	182.3
0.35		0.15	292.7	305.0	325.3	323.6
0.45	0.35		237.7	243.6	370.3	353.0
0.25			123.0	138.4	123.0	155.1
0.35		0.3	207.8	223.9	220.3	236.6
0.45			164.6	177.0	250.3	242.5

bridge piers made of SM570 and SM490, in which the energy absorption is defined as the area of the load-displacement envelope curve before the ultimate load point. Taking the analytical case in Fig. 5 as an example, the energy absorption of steel bridge pier made of SM570 is 293 MJ, which is almost equal to that of steel bridge pier made of SM490 (305 MJ). In other words, the steel bridge piers with SM570 and SM490 have close energy absorption capacity.

3.2 Effect of width-to-thickness ratio (R_f)

Fig. 7 illustrates the lateral load-lateral displacement envelope curves of steel bridge piers for different values of

R_f corresponding to $\bar{\lambda}$ = 0.25, 0.35, 0.45, P/P_y = 0.15 and 0.30, respectively. In which, Figs. 7(a) and (d), which have the smallest slenderness ratio, are selected to be studied. It is found from Fig. 7(a) that the ratio of ultimate load and yield lateral load (H_{max}/H_y) is 1.73, 1.57, 1.48, respectively, and the ratio of ultimate displacement and yield lateral displacement (δ_{max}/δ_y) is 8.0, 6.0, 4.0, respectively. From Fig. 7(d), H_{max}/H_y is 1.92, 1.73, 1.61, respectively, and δ_{max}/δ_y is 7.0, 5.0, 4.0, respectively. On one hand, it can be concluded that the ultimate load and its corresponding displacement increase with the decrease in R_f. On the other hand, larger P/P_y leads to larger H_{max}/H_y and smaller δ_{max}/δ_y. Clearly, the steel bridge piers with larger P/P_y have better ultimate load capacity and worse deformation capacity. Besides, the slope of post-buckling curve becomes steeper as R_f increases in both cases of $\bar{\lambda}$ = 0.35 and 0.45. Consequently, the parameter R_f has a great impact on the ultimate load and deformation capacities of the steel bridge piers.
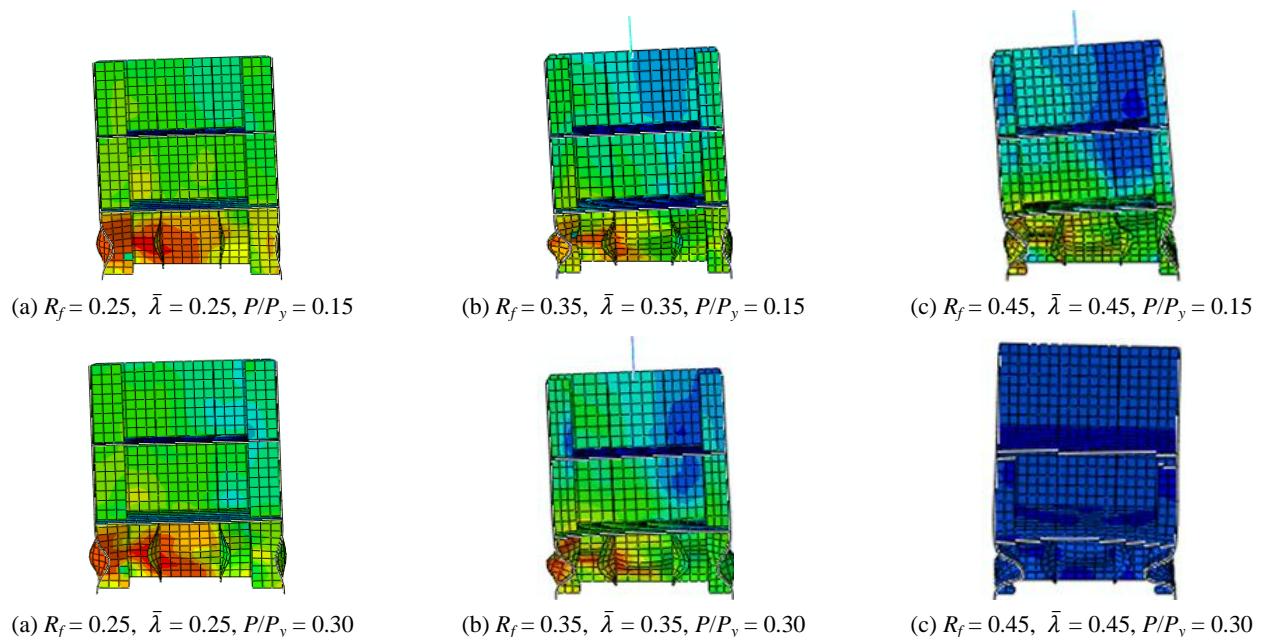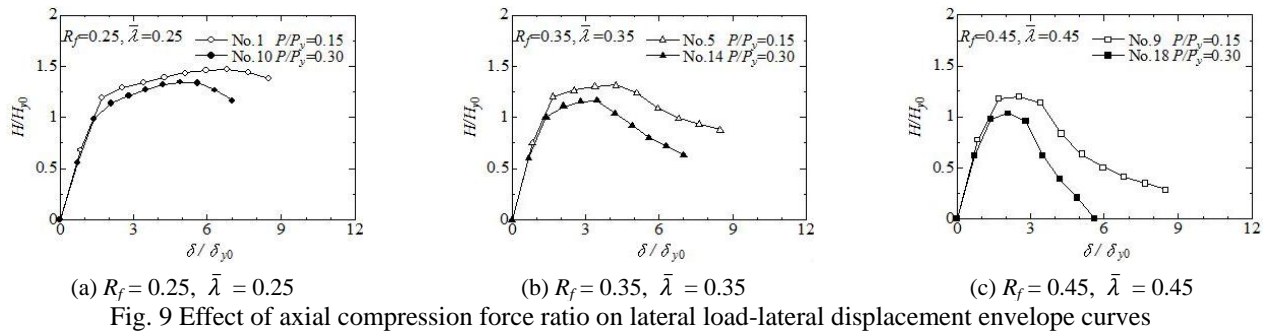
3.3 Effect of slenderness ratio ($\bar{\lambda}$)

Fig. 8 illustrates the lateral load-lateral displacement envelope curves of steel bridge piers for different values of

$\bar{\lambda}$ corresponding to R_f = 0.25, 0.35, 0.45, P/P_y = 0.15 and 0.30, respectively. In which, Figs. 8(a) and (d), which have the smallest width-to-thickness ratio, are selected to be studied. From Fig. 8(a), it is can be seen that H_{max}/H_y is 1.73, 1.69, 1.62, respectively, and δ_{max}/δ_y is 8.0, 7.0, 6.0, respectively. It is found from Fig. 8(d) that H_{max}/H_y is 1.92, 1.83, 1.71, respectively, and δ_{max}/δ_y is 7.0, 7.0, 6.0, respectively. Although both the ultimate load and deformation capacities increase with the decreasing of $\bar{\lambda}$ and the slope of post-buckling curve becomes smoother with the decrease of $\bar{\lambda}$, the effect of $\bar{\lambda}$ is much lower than that of R_f. Analytical results demonstrate that the steel bridge pier with a section of small width-to-thickness ratio and small column slenderness ratio exhibits a better seismic behavior of steel bridge piers, including ultimate load capacity and its corresponding deformation.

3.4 Effect of axial compression force ratio (P/P_y)

The effect of axial load on the seismic performance of steel bridge piers with stiffened box section is shown in Fig. 9. It should be observed that H_{y0} and δ_{y0} are employed to non-dimensionalize the curves. H_{y0} and δ_{y0} represent the yield lateral load and yield lateral displacement corres-

(a) R_f = 0.25, $\bar{\lambda}$ = 0.25   (b) R_f = 0.35, $\bar{\lambda}$ = 0.35   (c) R_f = 0.45, $\bar{\lambda}$ = 0.45

Fig. 9 Effect of axial compression force ratio on lateral load-lateral displacement envelope curves

(a) R_f = 0.25, $\bar{\lambda}$ = 0.25, P/P_y = 0.15   (b) R_f = 0.35, $\bar{\lambda}$ = 0.35, P/P_y = 0.15   (c) R_f = 0.45, $\bar{\lambda}$ = 0.45, P/P_y = 0.15

(a) R_f = 0.25, $\bar{\lambda}$ = 0.25, P/P_y = 0.30   (b) R_f = 0.35, $\bar{\lambda}$ = 0.35, P/P_y = 0.30   (c) R_f = 0.45, $\bar{\lambda}$ = 0.45, P/P_y = 0.30

Fig. 10 Local buckling deformation in analysis

ponding to the absence of axial load, respectively. These curves highlight the influence of axial load. As axial load increases, the ultimate load and its corresponding displacement decrease due to *P*-Δ effect.
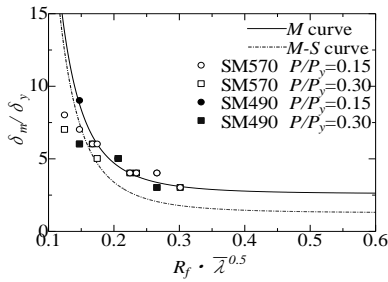
3.5 Local buckling deformation

Figs. 10(a)~(e) illustrate the local buckling deformation of the steel bridge piers made of SM570 at the end of analysis, which are affected by the main geometrical parameters and axial compression force ratio. Fig. 10(f) shows the local buckling deformation of pier during analysis because its analysis was not convergent. It is observed from Figs. 10(a) and (d) that the larger the value of P/P_y, the larger the local buckling deformation. Moreover, from Figs. 10(a), (b) and (c), the parameters R_f and $\bar{\lambda}$ have minor effect on the local buckling deformation of steel bridge piers.

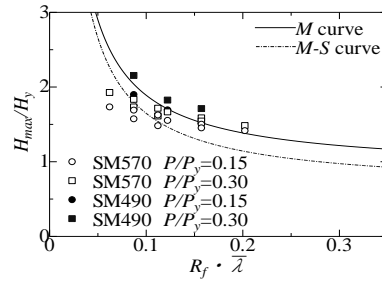## 4. Recommended formulas of ultimate load and deformation capacities in seismic design

Ultimate load and deformation capacities are important and necessary consideration in seismic design. First of all, the analytical results including ultimate load and deformation capacities are compared with the equations obtained from the reference (Usami *et al.* 2000). Then, the application scope of Eqs. (12)~(14) is obtained based on the tested results of reference (JRA 2002).

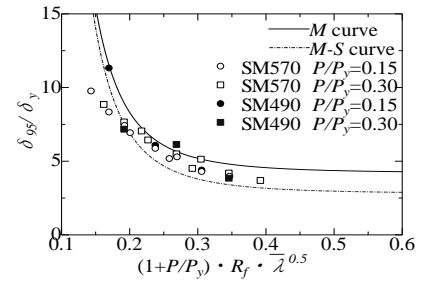$$\frac{H_{\max}}{H_y} = \frac{0.101}{R_f \bar{\lambda}} + 0.88 \qquad (S = 0.242) \quad (12)$$

$$\frac{\delta_{\max}}{\delta_y} = \frac{0.00759}{\left(R_f \sqrt{\bar{\lambda}}\right)^{3.5}} + 2.59 \qquad (S = 1.32) \quad (13)$$

$$\frac{\delta_{95}}{\delta_y} = \frac{0.0147}{\left\{\left(1 + P/P_y\right) R_f \sqrt{\bar{\lambda}}\right\}^{3.5}} + 4.20 \qquad (S = 1.40) \quad (14)$$

$$(0.3 \le R_f \le 0.7, 0.25 \le \bar{\lambda} \le 0.50,$$
$$0 \le P/P_y \le 0.2, \gamma / \gamma^* \ge 3.0)$$

where, *S* represents the standard deviation. The above equations are illustrated in Fig. 11, where *M* curve is average curve, and *M-S* curve is standard deviation curve. The solid line (*M* curve) in each plot denotes the plotted equations with average values of test results, while the dashed line (*M-S* curve) represents the curve which is lower than the solid line with a constant distance of *S*. It is observed that for the most part, the computed results are in good agreement with the fitted curves. However, when the value of $R_f\bar{\lambda}$ becomes small, the results obtained by the curves are higher (see Fig. 11(a)), especially for the steel bridge piers made of SM570.

Considering the influence of $\bar{\lambda}'_s$ on the ultimate load and deformation capacities of the steel bridge piers, the equations that provide satisfactory predictions to the computed results are fitted as follows in the reference (Usami *et al.* 2000)

$$\frac{H_{\max}}{H_y} = \frac{0.10}{\left(R_f \bar{\lambda} \bar{\lambda}'_s\right)^{0.5}} + 1.06 \qquad (S = 0.07) \quad (15)$$
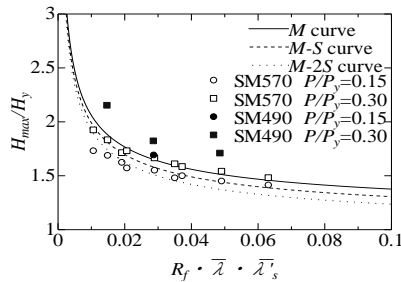

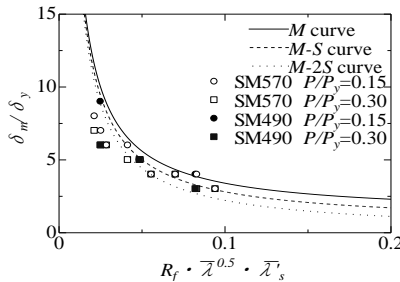(a) Analytical results and Eq. (12)   (b) Analytical results and Eq. (13)   (c) Analytical results and Eq. (14)
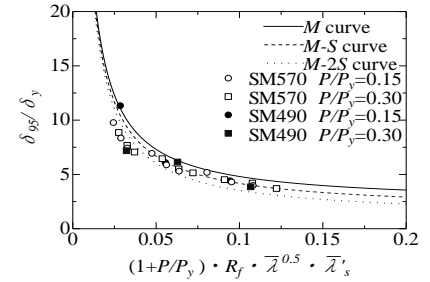
Fig. 11 Comparison between analytical results and approximate formula based on past experimental results

(a) Analytical results and Eq. (15)   (b) Analytical results and Eq. (16)   (c) Analytical results and Eq. (17)

Fig. 12 Comparison between analytical results and approximate formula based on past analytical results

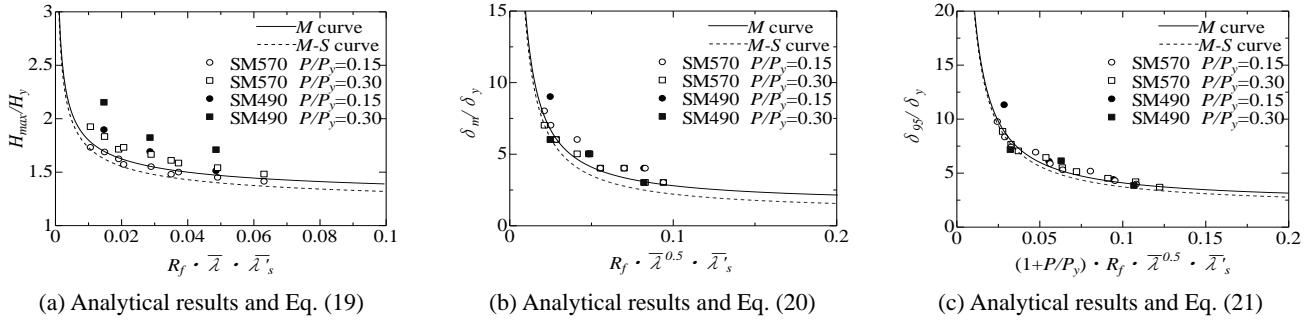(a) Analytical results and Eq. (19) (b) Analytical results and Eq. (20) (c) Analytical results and Eq. (21)

Fig. 13 Comparison between analytical results and proposed equations in this study

$$\frac{\delta_{max}}{\delta_y} = \frac{0.00759}{\left(R_f\sqrt{\overline{\lambda}}\,\overline{\lambda}'_s\right)} + 1.20 \qquad (S = 0.59) \qquad (16)$$

$$\frac{\delta_{95}}{\delta_y} = \frac{0.25}{\left(1+P/P_y\right)R_f\sqrt{\overline{\lambda}}\,\overline{\lambda}'_s} + 2.31 \qquad (S = 0.64) \qquad (17)$$

$$(0.25 \le R_f \le 0.56, \ 0.20 \le \overline{\lambda} \le 0.50,$$
$$0 \le P/P_y \le 0.3, \ \gamma/\gamma^* \ge 1.0)$$

where, the influence about aspect ratio of the flange plate between two diaphragms (α) on the slenderness ratio of stiffener ($\overline{\lambda}'_s$) is considered as

$$\overline{\lambda}'_s = \frac{1}{\sqrt[5]{\alpha}}\overline{\lambda}_s \qquad (18)$$

The above fitted equations are shown in Fig. 12. It can be obtained that the curves well represents the tendency with the variation of all the main parameters, although these predict equations still predict higher results in some cases.

In order to accurately predict the ultimate load capacity and deformation capacity of steel bridge pier made of SM570, the following new equations and corresponding application scope of them are obtained based analytical results in this study as following

$$\frac{H_{max}}{H_y} = \frac{0.06}{\left(R_f\overline{\lambda}\,\overline{\lambda}'_s\right)^{0.5}} + 1.20 \qquad (S = 0.07) \qquad (19)$$

$$\frac{\delta_{max}}{\delta_y} = \frac{0.13}{\left(R_f\sqrt{\overline{\lambda}}\,\overline{\lambda}'_s\right)} + 1.50 \qquad (S = 0.59) \qquad (20)$$

$$\frac{\delta_{95}}{\delta_y} = \frac{0.19}{\left(1+P/P_y\right)R_f\sqrt{\overline{\lambda}}\,\overline{\lambda}'_s} + 2.20 \qquad (S = 0.37) \qquad (21)$$

$$(0.25 \le R_f \le 0.45, \ 0.25 \le \overline{\lambda} \le 0.45,$$
$$0 \le P/P_y \le 0.3, \ \gamma/\gamma^* \ge 3.0)$$

The above fitted equations are plotted in Fig. 13, in which *M* curve is average curve, *M-S* curve is standard deviation curve and *M-2S* curve is variance curve. Compared to the existing empirical formulas, the proposed

formulas are more precise and more accurate within a certain range.

5. Comparison with predicted results

5.1 Comparison between tested results and predicted results

In this section, the proposed equations available for the steel bridge piers with stiffened box section made of SM570 will be validated by tested result in previous study. The cyclic test about stiffened box piers made of SM570 is lack, and only one tested case (KD-9) in the reference (Nakamura *et al.* 1997) is compared. Tested parameters and experimental results of KD-9 are listed in Table 4. Comparison between test results and presented equations in this study is illustrated in Fig. 14. The values of the maximum deformation and the 95% of maximum deformation obtained from proposed Eqs. (20) and (21) in this study agree well with the tested results, although the value of ultimate load obtained from Eq. (19) is higher than the tested ultimate load. Future validation experimental investigation is needed to further verify the effectiveness and availability of using proposed equations in this study to evaluate ultimate load capacity and deformation capacity of SM570 stiffened steel bridge piers.

5.2 Comparison between analytical results and predicted results

In order to validate the availability of proposed equations in this paper for the steel bridge piers under different axial compression force ratios, the analyses listed in Table 5 are conducted. The prediction results obtained from Eqs. (19)~(21) are in good agreement with analytical results in this section as shown in Fig. 15. It is concluded that the methodology adopting the Eqs. (19)~(21) can well predict the ultimate load and deformation capacities of HSS

Table 4 Tested parameters and experimental results

R_f	$\overline{\lambda}$	$\overline{\lambda}'_s$	P/P_y	H_y(tf)	δ_y (mm)
0.579	0.495	0.365	0.098	61.9	29.8
H_{max}(tf)	δ_m(mm)	δ_{95}(mm)	H_{max}/H_y	δ_m/δ_y	δ_{95}/δ_y
109	73.0	88.4	1.21	1.70	2.97

* Note: 1 tf = 9.8 kN

(a) Test results and Eq. (19)   (b) Test results and Eq. (20)   (c) Test results and Eq. (21)
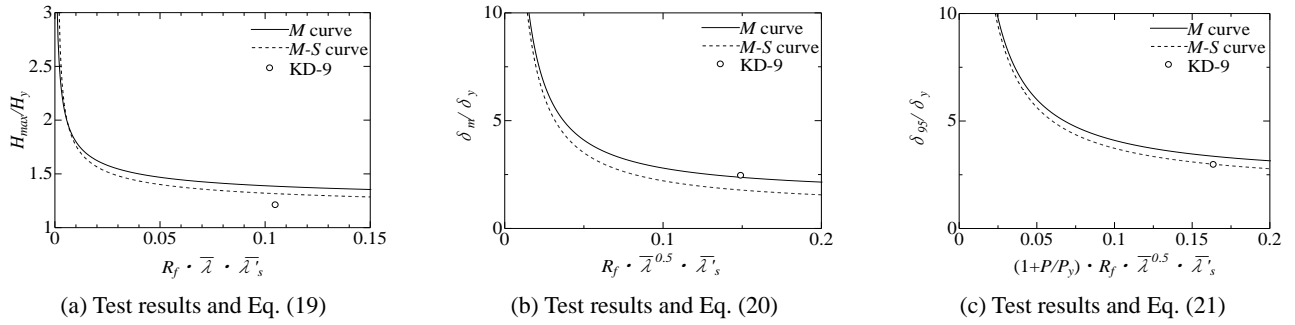
Fig. 14 Comparison between test result and proposed equations in this study

(a) Analytical results and Eq. (15)   (b) Analytical results and Eq. (16)   (c) Analytical results and Eq. (17)
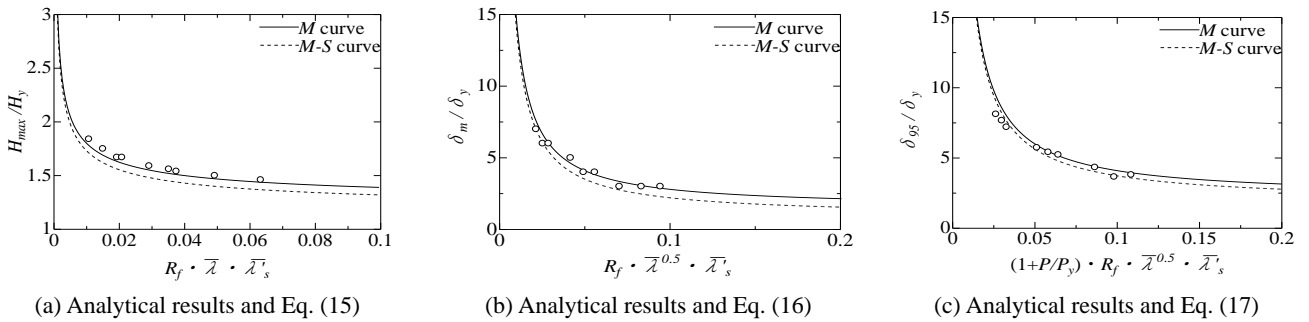
Fig. 15 Comparison between analytical results and proposed equations in this study

Table 5 Geometric dimensions and structural parameters of analytical steel bridge piers

No.	R_f	$\bar{\lambda}$	$\bar{\lambda}_s$	γ/γ^*	α	h (mm)	b (mm)	t (mm)	b_s (mm)	t_s (mm)	B (mm)	$\bar{t_f}$ (mm)	$\bar{t_w}$ (mm)	P/P_y	H_y (MN)	δ_y (mm)
25		0.25				2090								0.227	1.95	8.95
26	0.25	0.35	0.149			2926	625		92		645	23.30	29.99	0.175	1.47	16.77
27		0.45				3762								0.143	1.18	27.37
28		0.25				2968								0.231	2.64	12.93
29	0.35	0.35	0.207	3.0	0.50	4156	875	20	101	20	895	22.08	27.38	0.178	2.00	24.25
30		0.45				5343								0.145	1.60	39.60
31		0.25				3846								0.233	3.31	16.85
32	0.45	0.35	0.272			5384	1125		108		1145	21.86	25.95	0.180	2.50	31.61
33		0.45				6922								0.147	2.01	51.65

bridge piers with stiffened box section subjected to cyclic loading. In conclusions, the application ranges of proposed equations in this study are: the width-to-thickness ratio is from 0.25 to 0.45, the slenderness ratio is from 0.25 to 0.45, and the axial compression force ratio is from 0.0 to 0.3.

6. Conclusions

Based on the parametric analyses of SM570 and SM490 steel bridge piers with stiffened box section under cyclic loading, some formulas for predicting the ultimate load capacity and deformation capacity of steel bridge piers made of SM570 are proposed. The influences of steel type, width-to-thickness ratio, slenderness ratio, axial compression force ratio on the seismic performance of steel bridge

piers are investigated. Based on the numerical results, the main following conclusions consist of:

- The effect of steel type on the seismic behavior of steel bridge piers under regular cyclic loading is investigated. The steel bridge piers made of SM570 have higher ultimate load capacity, but worse deformation capacity. The energy absorption of steel bridge piers made of SM570 is almost equal to that of steel bridge piers made of SM490.
- The effect of width-to-thickness ratio on the deformation capacity of steel bridge pier made of SM570 is more obvious than that of slenderness ratio on the deformation capacity.
- It can be noted that for the most cases, the analytical results agree well with the existing fitted curves in

the previous studies on NSS piers. But, when the value of horizontal axis becomes small, results obtained from the curves are higher, especially for the steel bridge piers made of SM570.

- The formulas for predicting the ultimate load capacity and deformation capacity of stiffened steel bridge box piers made of SM570 are presented. Compared to the existing empirical formulas, the proposed formulas are more precise and accurate because they incorporate the main influence factors that affect the ultimate load and deformation capacities of such steel bridge box piers.

Acknowledgments

References

Aoki, T. and Susantha, K.A.S. (2005), "Seismic performance of rectangular-shaped steel piers under cyclic loading", *J. Struct. Eng. ASCE*, **131**(2), 240-249.

Japan Road Association (2002), *Specifications for highway bridges*, *Part V*, *seismic design*, Tokyo, Japan.

Ban, H., Shi, G., Shi, Y. and Bradford, M.A. (2013a), "Experimental investigation of the overall buckling behaviour of 960 MPa high strength steel columns", *J. Constr. Steel Res.*, **88**, 256-266.

Ban, H.Y., Shi, G., Bai, Y., Shi, Y.J. and Wang, Y.Q. (2013b), "Residual stress of 460 MPa high strength steel welded I section: Experimental investigation and modeling", *Int. J. Steel Struct.*, **13**(4), 691-705.

Ban, H.Y., Shi, G., Shi, Y.J. and Bradford, M.A. (2013c), "Experimental investigation of the overall buckling behaviour of 960 MPa high strength steel columns", *J. Constr. Steel Res.*, **88**, 256-266.

Bradford, M.A. and Liu, X.P. (2016), "Flexural-torsional buckling of high-strength steel beams", *J. Constr. Steel Res.*, **124**, 122-131.

Cao, K., Guo, Y.J. and Zeng, D.W. (2015), "Buckling behavior of large-section and 420 MPa high-strength angle steel columns", *J. Constr. Steel Res.*, **111**, 11-20.

Chen, S.W., Chen, X., Wang, Y.B., Lu, Z.L. and Li, G.Q. (2016), "Experimental and numerical investigations of Q690D H-section columns under lateral cyclic loading", *J. Constr. Steel Res.*, **121**, 268-281.

Chiew, S.P., Jiang, J. and Lee, C.K. (2012), "Residual stress investigation of welded high strength steel box T-joints", *Elect. Measur. Instru. Measur.*, **177**, 141-147.

Coelho, A.M.G. and Bijlaard, F.S.K. (2010), "Finite element evaluation of the strength behaviour of high-strength steel column web in transverse compression", *Steel Compos. Struct., Int. J.*, **10**(5), 385-414.

Ferrario, F., Iori, F., Pucinotti, R. and Zandonini, R. (2016), "Seismic performance assessment of concentrically braced steel

frame buildings with high strength tubular steel columns", *J. Constr. Steel Res.*, **121**, 427-440.

Gao, L., Sun, H., Jin, F. and Fan, H. (2009), "Load-carrying capacity of high-strength steel box-sections I: Stub columns", *J. Constr. Steel Res.*, **65**(4), 918-924.

Ge, H.B. and Kang, L. (2012), "A damage index based evaluation method for predicting the ductile crack initiation in steel structures", *J. Earthq. Eng.*, **16**(5), 623-643.

Ge, H.B., Gao, S.B. and Usami, T. (2000), "Stiffened steel box columns. Part 1: Cyclic behaviour", *Earthq. Eng. Struct. Dyn.*, **29**(11), 1691-1706.

Gkantou, M., Theofanous, M., Wang, J., Baniotopoulos, C. and Gardner, L. (2017), "Behaviour and design of high-strength steel cross-sections under combined loading", *Proceedings of the Institution of Civil Engineers-Structures and Buildings*, **170**(11), 841-854.

Guo, W., Crowther, D., Francis, J.A., Thompson, A., Liu, Z. and Li, L. (2015), "Microstructure and mechanical properties of laser welded S960 high strength steel", *Mater. Des.*, **85**, 534-548.

Joo, H.S., Moon, J., Sung, I.-H. and Lee, H.-E. (2015), "Moment redistribution of continuous composite I-girder with high strength steel", *Steel Compos. Struct., Int. J.*, **18**(4), 873-887.

Khan, M., Paradowska, A., Uy, B., Mashiri, F. and Tao, Z. (2016), "Residual stresses in high strength steel welded box sections", *J. Constr. Steel Res.*, **116**, 55-64.

Kumar, S. and Usami, T. (1996), "Damage evaluation in steel box columns by cyclic loading tests", *J. Struct. Eng. JSCE*, **122**(6), 626-634.

Li, T.J., Li, G.Q., Chan, S.L. and Wang, Y.B. (2016a), "Behavior of Q690 high-strength steel columns: Part 1: Experimental investigation", *J. Constr. Steel Res.*, **123**, 18-30.

Li, T.J., Liu, S.W., Li, G.Q., Chan, S.L. and Wang, Y.B. (2016b), "Behavior of Q690 high-strength steel columns: Part 2: Parametric study and design recommendations", *J. Constr. Steel Res.*, **122**, 379-394.

Li, D., Uy, B., Patel, V. and Aslani, F. (2017), "Analysis and design of demountable embedded steel column base connections", *Steel Compos. Struct., Int. J.*, **23**(3), 303-315.

Liao, F.-Y., Han, L.-H., Tao, Z. and Rasmussen, K.J.R. (2017), "Experimental behavior of concrete-filled stainless steel tubular columns under cyclic lateral loading", *J. Struct. Eng.*, **143**(4), 04016129.

Ma, J.-L., Chan, T.-M. and Young, B. (2016), "Experimental investigation of cold-formed high strength steel tubular beams", *Eng. Struct.*, **126**, 200-209.

Mamaghani, I.H.P., Shen, C., Mizuno, E. and Usami, T. (1995), "Cyclic Behavior of Structural Steels. I: Experiments", *J. Eng. Mech. ASCE*, **121**(11), 1158-1164.

Nakamura, S., Yasunami, H., Kobayashi, B., Nakagawa, T. and Mizutani, S. (1997), "An experimental study on the seismic performance of steel bridge piers with less-stiffened and compact sized section", *Proceedings of Nonlinear Numerical Analysis and Seismic Design of Steel Bridge Piers*, pp. 331-338.

Nakashima, M. and Liu, D.W. (2005), "Instability and complete failure of steel columns subjected to cyclic loading", *J. Eng. Mech. ASCE*, **131**(6), 559-567.

Shen, C., Mamaghani, I.H.P., Mizuno, E. and Usami, T. (1995), "Cyclic behavior of structural steels. II: Theory", *J. Eng. Mech. ASCE*, **121**(11), 1165-1172.

Shi, G., Liu, Z., Ban, H.Y., Zhang, Y., Shi, Y.J. and Wang, Y.Q. (2012), "Tests and finite element analysis on the local buckling of 420 MPa steel equal angle columns under axial compression", *Steel Compos. Struct., Int. J.*, **12**(1), 31-51.

Shi, G., Zhou, W.J., Bai, Y. and Liu, Z. (2014), "Local buckling of steel equal angle members with normal and high strengths", *Int. J. Steel Struct.*, **14**(3), 447-455.

Shi, G., Zhou, W.J. and Lin, C.C. (2015), "Experimental

Investigation on the Local Buckling Behavior of 960 MPa High Strength Steel Welded Section Stub Columns", *Adv. Struct. Eng.*, **18**(3), 423-437.

Usami, T. and Ge, H.B. (1998), "Cyclic behavior of thin-walled steel structures--numerical analysis", *Thin-Wall. Struct.*, **32**(1-3), 41-80.

Usami, T., Gao, S.B. and Ge, H.B. (2000), "Stiffened steel box columns. Part 2: Ductility evaluation", *Earthq. Eng. Struct. Dyn.*, **29**(11), 1707-1722.

Wang, Z.F. and Yamao, T. (2011), "Ultimate strength and ductility of stiffened steel tubular bridge piers", *Int. J. Steel Struct.*, **11**(1), 81-90.

Wang, J.J., Shi, G. and Shi, Y.J. (2014a), "Experimental research on behavior of 460 MPa high strength steel I-section columns under cyclic loading", *Earthq. Eng. Eng. Vib.*, **13**(4), 611-622.

Wang, Y.B., Li, G.Q., Cui, W. and Chen, S.W. (2014b), "Seismic behavior of high strength steel welded beam-column members", *J. Constr. Steel Res.*, **102**, 245-255.

Wang, Y.B., Li, G.Q., Cui, W., Chen, S.W. and Sun, F.F. (2015), "Experimental investigation and modeling of cyclic behavior of high strength steel", *J. Constr. Steel Res.*, **104**, 37-48.

Wang, J., Afshan, S., Gkantou, M., Theofanous, M., Wang, J. and Gardner, L. (2017a), "Flexural buckling of hot-finished high-strength steel SHS and RHS columns", *J. Struct. Eng.*, **143**(6), 04017028.

Yan, J.-B., Liew, J.Y.R., Zhang, M.-H. and Wang, J.-Y. (2014), "Mechanical properties of normal strength mild steel and high strength steel S690 in low temperature relevant to Arctic environment", *Mater. Des.*, **61**, 150-159.

Zheng, Y., Usami, T. and Ge, H.B. (2000), "Ductility evaluation procedure for thin-walled steel structures", *J. Struct. Eng. ASCE*, **126**(11), 1312-1319.

BU